NUMERICAL STUDY OF ENERGY UTILIZATION IN NOZZLE/PLUME FLOW-FIELDS OF HIGH-SPEED AIR-BREATHING VEHICLES

Dr. David Riggins
Missouri University of Science & Technology

Dr. David Moorhouse
United States Air Force Research Laboratory

Ms. Althea Wilson
Missouri University of Science & Technology

Keywords: hypersonics, propulsion, aircraft design

Abstract

Focused local energy deposition in both internal and external flow-fields associated with high-speed aerospace vehicles can provide many system level benefits. This study specifically analyzes the effects of targeted (local) energization of the flow in the nozzle and afterbody flow-field regions of a sub-scale hypersonic lifting body configuration. Benefits are shown to include the generation of a favorable vehicle pitching moment (nose-down) increment associated with such energy deposition and a reduced local and overall thermal load in both combustor and nozzle for all cases examined. These results have been obtained by modeling the nozzle/afterbody region of a simple generic 2-D wave-rider/lifting body utilizing computational fluid dynamics (CFD). In these simulations energy was deposited locally in the flow-field; energy location, amount, and the shape and extent of the energized zone were then parametrically varied. Force distributions were then integrated to obtain overall axial force contributions and moment effects on the vehicle surfaces modeled; these are compared to the baseline (i.e. the configuration with no nozzle/afterbody energization). The distribution of the temperature on the adiabatic nozzle/afterbody wall surface (which serves as an indicator of thermal load effects on the

vehicle) is also examined. It is shown that by optimal placement of a single intense energy deposition, increases in the overall engine nose-down moment of 50-125% and reductions of up to 500 K in the wall temperature distribution throughout the nozzle/afterbody region of the engine can be achieved. There are penalties in the overall engine thrust (axial force) production of 15-20% when energy is added other than in the combustor (due to the inevitable reduction in thermal efficiency), however it is conjectured based on the results of this preliminary study that the overall system benefits (favorable moment effects and reduced heating loads) may to some degree outweigh these propulsive penalties in order to allow for optimization of the entire vehicle.

1 Introduction

Hypersonic air-breathing vehicles have the potential to dramatically expand and improve flight capability for many applications. Such vehicles will facilitate rapid global reach capability for both civilian and military purposes and will allow more affordable and reliable access-to-space missions. The hypersonic flight regime has many challenges due in part to the strong shock waves and high pressures and temperatures associated with hypersonic flow. One of the design configurations examined for use in this regime

is the lifting body/wave-rider. This configuration has been successfully modeled, tested, and flown [1], [2] and [3]. (Note that the X-43 HyperX vehicle is undoubtably the most well-known and recent example.) Vehicles which are based on the lifting body/wave-rider concept have generally favourable characteristics for hypersonic flight, including relatively low drag and the generation of considerable lift from the forebody shock wave and the afterbody nozzle expansion process (i.e. favourable L/D ratios). Nevertheless, such configurations also present significant engineering challenges due to a number of issues including high heat transfer, particularly in the propulsion system (requiring complex and heavy active cooling sub-systems within the combustor), and problems with vehicle stability and control. Of specific interest here is the inherent nose-up pitching moment for this class of vehicles. This moment results from the natural distribution of pressure and shear forces over the wetted surfaces at hypersonic Mach numbers as well as the necessary packaging of on-board systems as allowed within the general shape characteristic of the configuration. For instance, the X-43 vehicle required a large tungsten mass of 800 lbs located in the nose (representing 26% of the overall mass); this mass was mainly necessary simply in order to counter this unfavourable moment. This issue is an obvious major liability for this type of vehicle (although it is mitigated in part for larger scale vehicles). The purpose of the present study is to investigate a possible method for decreasing the heat transfer (by distributing the energy release through both combustor and nozzle systems) and simultaneously significantly reducing the inherent nose-up pitching moment of this class of vehicle by the generation of a stronger nose-down moment in the nozzle/afterbody.

A technique that can be used to modify flow fields around and adjacent to the vehicle (and in the propulsion system) and hence impact vehicle performance is localized (or targeted) energy deposition [4]-[11]. Conventional thought in high-speed vehicle design dictates that the energy addition take place (to the maximum degree possible) in the combustor since this location corresponds to the highest thermal efficiency, due to the lower Mach number and resulting high pressures and temperatures. However, previous studies have shown that small amounts of flow energization in front of the vehicle (i.e. by the use of microwaves) can have a large impact on the external flow-field by modifying the shock structure which in turn can cause a significant drag reduction. The so-called power effectiveness of such techniques (drag power savings divided by the power needed for the flow-field modification) can be extremely large. Similarly, energy added just upstream and beneath the cowl leading edge can generate an increase in the mass flow rate of air captured by the engine. In addition, energy can be added adjacent to external surfaces of the vehicle thus enabling the ability to control the vehicle through non-mechanical interactions. The concept of using focused energy deposition to modify the flow adjacent to or inside of an aerospace vehicle views energy management properly from the standpoint of the entire system, rather than from only the propulsion sub-system [12].

The current study was performed in order to investigate possible beneficial effects of distributed (or targeted) flow energization in the nozzle and/or afterbody flow-fields of a vehicle. Therefore, in this work a small (15-30%) portion of the on-board energy is purposely withheld from the combustor and is instead utilized in the nozzle/afterbody region of the vehicle; the resultant changes in propulsion flow-path/vehicle performance are then examined. This is accomplished by performing a parametric two-dimensional numerical (CFD) investigation of the impact of localized energy deposition in the nozzle/aftbody region of a lifting body hypersonic configuration. Of particular interest in this study are the vehicle moments generated by utilizing this concept as well as possible reductions in the thermal loading of the vehicle structure. As mentioned earlier, stability and control and heat transfer are major challenges for high speed aerospace vehicle designs and

hence a technique that addresses both these challenges simultaneously would be attractive for further analysis. Figure 1.1 below provides an illustration of the general concept of innovative energy management for high speed vehicles and shows some possible (non-traditional) uses of energy within the flowpaths around and through the vehicle. Previous studies have examined the impact of energy deposition for drag reduction, mass capture and non-mechanical control, and the specific focus of the current investigation is the impact of distributed energy in the propulsion system, with emphasis on its placement/distribution in the nozzle/afterbody flow-field of the vehicle.

Energy addition in locations other than the combustor will inevitably lower the actual thrust of the propulsion system since there is a reduction in thermal efficiency due to the addition of heat at lower temperatures and pressures. However, by depositing the energy appropriately in the nozzle, some axial force contributing to overall thrust can nevertheless possibly be recovered by local pressurization of the nozzle walls. This effect is both through thermodynamic pressurization caused by the heating (one-dimensional effects) as well as by possible compression/shock wave interactions emanating from the heated zone and intersecting the wall regions (multi-dimensional effects). This is due to the fact that for energy deposition which is sufficiently intense, compression waves can actually coalesce into a shock wave in the vicinity of the energization which ultimately can pressurize the walls.

It is also possible that the heat transfer to the combustor/nozzle wall surfaces themselves can be significantly reduced. This may result since (although the energy deposition will heat the flow in the local zone) the heated gas may be entrained in the main flow of the nozzle and swept out of the nozzle and into the wake before the heat can be convected to solid nozzle/afterbody surfaces. The compression waves/shock system from the heated zone, however, can impact the walls and generate thrust contributions as discussed above. Figure 1.2 illustrates the physics of the

concept for a generic scenario in which there is partial thrust recovery from intense energy deposition but accompanied by (possibly) significantly reduced heat transfer as measured relative to the case in which all energy is added in the combustor.

The susceptibility of the flow at the wall to fluid-dynamic separation due to the adverse pressure gradient associated with the compression/shock structure emanating from the heated zone is also of obvious importance in such a study; separation will reduce nozzle performance and lead to possible high transfer rates locally in the affected zones. However, the overall favourable pressure gradient in the nozzle/afterbody region of the vehicle will tend to inhibit separation to some extent. This study utilizes laminar flow which is more prone to separation and will provide a preliminary assessment of this issue.

Finally, the shock wave produced by the energy deposition can also induce a significant nose-down pitching moment contribution on the vehicle in the context of a wave-rider/lifting body nozzle/afterbody, if the energy is appropriately deposited far enough downstream in the nozzle. This moment is due to pressurization of (body-side) nozzle/afterbody surfaces far aft of the combustor, i.e. such that there is a significant moment arm for the resultant force (as measured from the vehicle center of gravity, cg), as depicted schematically in Figure 1.3.

Localized energy deposition can be accomplished in a number of different ways. Microwaves and/or lasers can be targeted to heat a specific zone. Injection of a secondary flow or plasma generation in the flow can also be used for targeted energy deposition. All of these methods have been previously (and more or less successfully) examined for upstream energy deposition and also for facilitating ignition within combustors; the concept of nozzle energy deposition, however, also presents another possibility in terms of utilizing chemical combustion. Depending on the desired location(s) for nozzle energy deposition, it may be possible to inject a relatively small amount of fuel from the nozzle
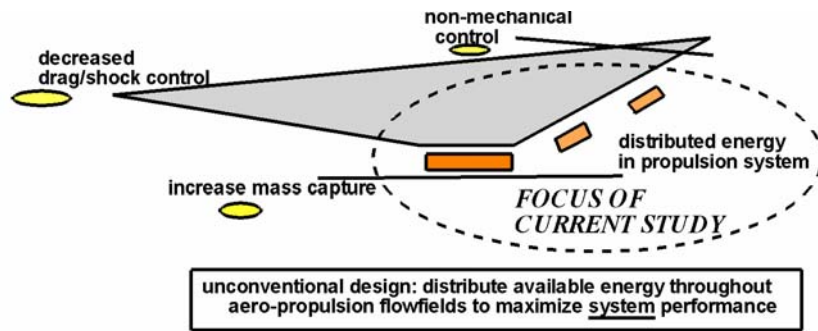
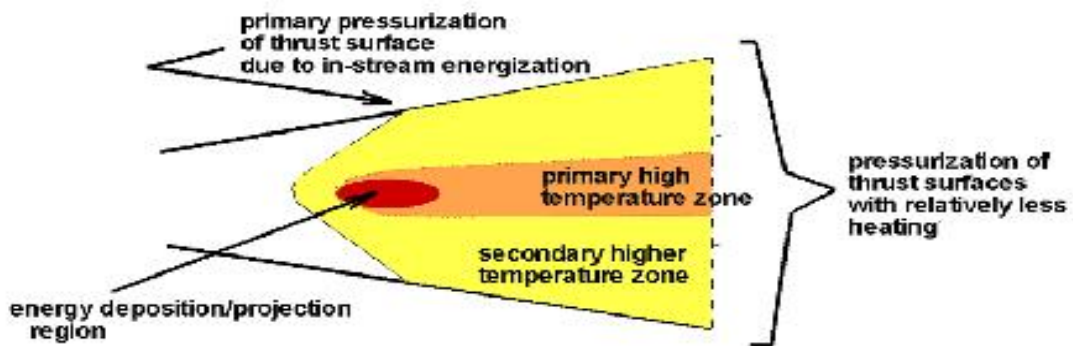Fig. 1.1. Energy management for optimal performance high-speed vehicles

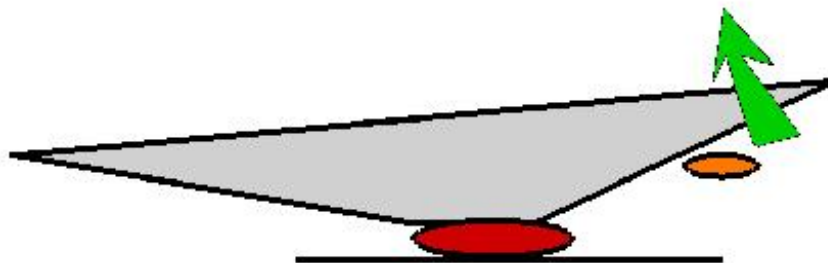Fig.1.2. Temperature effects induced by local energy deposition in nozzle/aftbody flow-fields

Fig.1.3. Moment effects induced by local energy deposition in nozzle/aftbody flow-fields

wall and ignite it (possibly utilizing microwaves if necessary) resulting in a local 'deposition' of heat release in the flow.

Alternatively, if the engine has incomplete combustion, which is common for high speed engines in which the combustion is mixing-limited within the combustor itself, it may be possible to simply ignite fuel already entrained (and mixed) in the nozzle flow. This, however, is highly dependent on the flow characteristics and would probably be harder to target to a specific desired region.

For the purposes of the current study, it was considered sufficient to model the energy deposition as a source term in the energy equation; this corresponds in terms of energization to the utilization of microwaves and/or lasers (addition of heat). This method is the simplest method of modelling the energy deposition for such a preliminary study and avoids the complications of modelling injection or chemical interactions.

The organization of this paper is as follows: The first main section (the current section) provides a general discussion of the relevant topics of focused energy deposition and a parallel discussion of the challenges presented by hypersonic flight and the context and objectives of the present investigation. Section 2 provides an overview of the methodology (approach taken) for the parametric study of energy deposition in nozzle/afterbody regions while Section 3 gives some details of the CFD code, geometry of vehicle, and computational grid used in the study. Section 4 gives specifics on the models used, i.e. how the inlet, combustor and nozzle/afterbody were modeled and how the forces and moments were calculated. Section 5 discusses the results of the numerical simulations of the combustor and nozzle and reviews the effects of varying different parameters in the nozzle energy deposition. Section 6 discusses the analysis of the moments and forces for the forebody and the impact on the overall propulsion flowpath. Section 7 provides estimation of some system-level effects in terms of an effectiveness of the energy deposition, based on the results

obtained in this paper. Finally, Section 8 concludes the paper by summarizing the main results and provides suggestions of future work necessary to further examine the concept of distributed energy in high-speed air-breathing flowpaths.

2 Methodology

This section provides a summary of the methodology and approach that was taken to study the effects of energy deposition in nozzle/afterbody flow-fields. Both conventional (all heat added in the combustor) and a selection of unconventional (nozzle flow-field distributed energy) configurations were analyzed in order to quantify the performance effects of interest.

The study utilized air throughout the engine with thermal heating via a source term in the energy equation to model both combustor heat release (chemical combustion) as well as localized heat release (energy deposition) downstream in the nozzle. The base energy rate (always) added into the combustor was taken as five megawatts, which (for the very sub-scale configuration examined in this study) corresponded to the energy rate equivalent released by combustion of 0.042 kg/s of H_2 in air (H_2-air heating value $= 1.2 \times 10^8$ J/kg). This then gives a fuel-air mass ratio of 0.0157, corresponding to 54% of the stoichiometric value of 0.029. However, the total energy added to the flow in both combustor and nozzle was then varied between six and seven megawatts, with the parametric study focusing on various splits (portioning) of the additional one to two megawatts of energy between the combustor and the nozzle regions. Six megawatts of total energy rate corresponds to the energy rate equivalent associated with 60% of stoichiometric while seven megawatts corresponded to 70% of stoichiometric. The range of energy rates for unconventional cases (in which the total energy rate added into the flow was split between nozzle and combustor) varied such that between 70-85% of the total energy rate was put into the combustor and 15-

30% of the total energy rate was added in small focused zones within the nozzle.

The methodology for this study consisted first of an analytical treatment of the inlet/combustor (in which various combustor exit conditions corresponding to the various desired amount of energy release were generated). This analytical treatment was followed by an extensive parametric two-dimensional CFD study which provided the flow-fields (and ultimately force, moment, and thermal performance) for the nozzle/afterbody region with varying parameters for the distributed energy deposition. The CFD simulations generated in this (second) part of the investigation then simply defined the inflow boundary conditions into the nozzle as the combustor exit conditions that were determined analytically in the first part of the investigation.

As noted above, the parametric CFD study focused on the 2-D numerical simulation of a zone encompassing the nozzle/afterbody region of the flow-field including the flow underneath the cowl as outlined by the blue box shown in Figure 2.1. This region was simulated using CFD; the inflow into the computational domain underneath the cowl was assumed to have conditions corresponding to freestream. The combustor outflow conditions, as noted above and which served as the inflow to the upper portion of the modelled zone were found analytically via control volume analysis of the combustor/inlet, as described subsequently.

The parametric study simulated the nozzle/afterbody flow field for studies of energy deposition (both conventional and non-conventional) and then post-processed the (integrated) distribution of the pressure forces on the surfaces of the nozzle/afterbody in order to compute the overall force and moment experienced by the modelled surfaces of the vehicle for various cases to be described subsequently. The shear force was not considered since the laminar modelling of the flow meant that the shear contribution was small.

After the parametric study was completed, the associated vehicle forebody/inlet flow-fields were examined (analytically) using the moment-of-momentum theorem to estimate the pitching moment on that part of the propulsive flowpath; this then allowed estimations of the forces and moments for the entire propulsive flow-path. For the present study, the weight of the vehicle was not estimated as it was not needed for the specific objectives of the current study. Furthermore, the effects of the wing or lifting surfaces were not considered; such that this study only examined the illustrated cross-section of the vehicle, i.e. that part of the flow corresponding to the propulsion system including energy deposition, the upper surface shock system, and the plume expansion process (as modelled using the CFD). Note, however, that system-level benefits must be eventually assessed such that vehicle weight and lifting surfaces should be coupled with the present analysis to provide true system-level analysis of the techniques explored in this study.

3 Geometry, CFD Code and Grid for Parametric Study

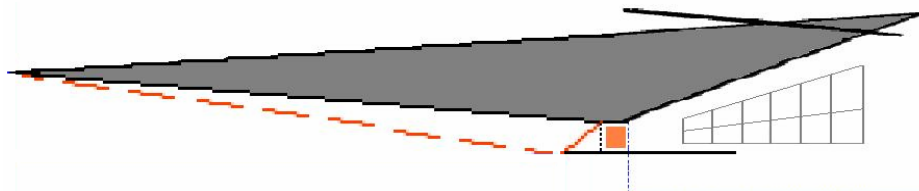The parametric CFD study defined the domain for computations as the nozzle and

Fig. 2.1. Vehicle cross-section showing control volume and nozzle energy deposition grid used for parametric (location of energy deposition) study

afterbody region of a sub-scale (2-D) vehicle (see Figure 2.1). The cowl was modelled as a thin rectangular surface which separated the combustor flow from the free-stream (bottom) flow until the mixing of the two streams with subsequent plume effects occurs at cowl trailing edge. Note that the vehicle for the purposes of this work is considered to be at zero angle of attack (there is therefore no deviation from free-stream conditions for the inflow used beneath the cowl). This assumption has a significant effect on the measured moments.

This investigation used the SPARK explicit finite-difference CFD code which is a 2-D Navier-Stokes (laminar) time-marching code that was originally developed at NASA Langley for the simulation of high-speed propulsive flow-paths [13]. It utilizes a variable specific heat model and has the ability to handle chemical reactions, although this study as constructed did not model reacting flows. The thermodynamic curve fits used in the code are only valid at temperatures below 5500K, so any cases that exceeded that temperature were eliminated from the matrix. The energization within the nozzle was accomplished by incorporating a source term within the energy equation; this then corresponds to simple direct deposition of energy (as heat) into the targeted zone. The use of the laminar model in the code (rather than modelling the flow as turbulent) should

not greatly affect the bulk performance effects to be examined by the energy deposition techniques that are examined here with the following caveats: first, the susceptibility to separation on the walls of the nozzle/afterbody will be increased by laminar flow modelling (over that expected in turbulent flow) due to the lower momentum fluid elements near the wall. For that, then, the present study is conservative, i.e. should show more severe separation tendencies than what would be expected in actual turbulent flow. However, turbulent flow can be expected to significantly increase thermal diffusion from heated zones – this increase in thermal diffusion may result in increased wall heating loads than indicated in the present study.

The baseline computational grid used in this study is rectangular with 401 nodes in the x-direction and 201 nodes in the y-direction as shown in Figure 3.1. It encompasses the nozzle/afterbody, truncated cowl and free-stream flow underneath the cowl in order to capture the plume and nozzle flow-field characteristics and interactions in the flow. The nozzle is 0.20 m long and the height is 0.095 m measured from the cowl to the nozzle trailing edge, the cowl is truncated 0.05 m after the combustor exit which results in the nozzle exhaust interacting with the flow underneath the body. The grid is clustered in the y-direction near the top wall and at the cowl; it is also clustered in the x-direction near the end of
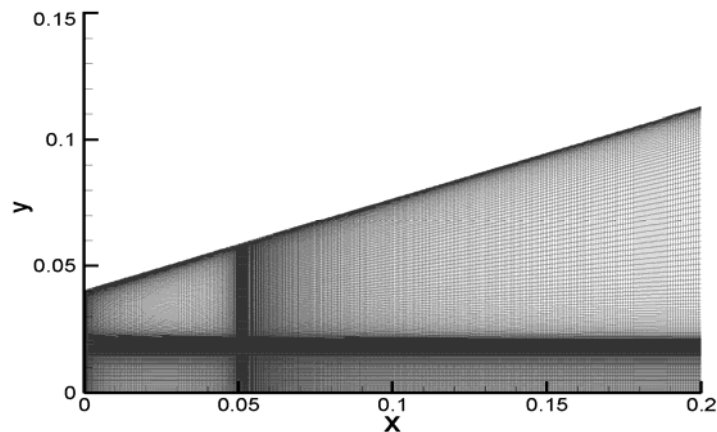

Fig. 3.1. CFD grid

the cowl. At the inflow to this simulated region, the combustor outflow (top) is 0.02 m high and free-stream inflow boundary under the cowl is 0.02 m high. The cowl solid structure is an embedded boundary within the grid with a constant thickness of 0.0003 m. Wall conditions were handled as no-slip and adiabatic for all solid surfaces. Combustor outflow conditions as computed analytically (described subsequently in Section 4.2) were used for the top inflow to the modelled zone; free-stream conditions were assumed below the cowl on modelled zone inflow. Flow at the outflow and lower boundaries for the computational zone were extrapolated. Note that the energy addition within the nozzle was modelled as occurring in zones defined along grid lines; i.e. for this study the shape of the energized zones simply overlaid the defined grid.

4. Analysis Description

4.1 Forebody Analysis

The freestream conditions utilized for this study corresponded to Mach 9 flight at 30 km altitude (i.e. static pressure and temperature equal to 1185 N/m^2 and 231.24K, respectively) and zero vehicle angle of attack. The inlet (engine) face height was taken as 0.05412 meters such that the mass flow rate of air inducted into the engine is then 2.6592 kg/sec. The inlet exit (combustor entrance) is taken as 0.02m. This yields a very small inlet contraction ratio of less than 3.0 (for this flight Mach number a significantly higher contraction ratio may be expected on an actual flight vehicle). However this contraction ratio is considered sufficient for the purpose of the current study which is primarily interested in the effect of energy distribution in the nozzle/afterbody regions of the vehicle. An inlet total pressure recovery of 0.078 (corresponding to a $\Delta S / R = 2.5533$) was used along with the assumption of an adiabatic inlet (i.e. total enthalpy flow rate into combustor equals engine inflow total enthalpy flow rate). These assumptions then enable the direct

analytical calculation of the inlet exit (or combustor entrance conditions) $P_{ci}, T_{ci}, \rho_{ci}, u_{ci}$ from the following four relations (gas equation of state, continuity, energy equation, and entropy considerations):

$$P_{ci} = \rho_{ci} R T_{ci} \qquad (1)$$

$$\rho_i u_i A_i = \rho_{ci} u_{ci} A_{ci} \qquad (2)$$

$$\left\{ \sum_{l=1}^{ncs} \alpha_l (h_{ref,l} + \int_{T_{ref}}^{T_i} C_{P,l} dT) \right\} + \frac{u_i^2}{2} =$$

$$\left\{ \sum_{l=1}^{ncs} \alpha_l (h_{ref,l} + \int_{T_{ref}}^{T_{ci}} C_{P,l} dT) \right\} + \frac{u_{ci}^2}{2} \quad (3)$$

$$s_i + \Delta s = s_{ci} \qquad (4)$$

where $s = \sum_{\ell=1}^{NCS} \alpha_\ell s_\ell$ and

$$s_\ell = s_{o\ell} + \int_{T_{ref}}^{T} C_{p\ell} \frac{dT}{T} - r_\ell \frac{P}{P_{ref}} \qquad (5)$$

$s_{o\ell}$ = reference entropy at T_{ref}, P_{ref} of species ℓ

r_ℓ = gas constant for species ℓ

Note that all coefficients for the thermodynamics (specific heat polynomial modelling) and reference enthalpies and entropies are taken from the Gordon-McBride curve fits [14]. Air composed of 76.86% N2 and 23.14% O2 was used in this study such that a constant specific gas constant of 288.22 J/kgK results. This analytical approach as described here did not require the detailed modelling of the inlet; however, future studies should incorporate CFD modelling and simulation of the inlet itself as well as angle of attack effects. The combustor inflow conditions obtained utilizing this analysis is therefore as follows:

$P_{ci} = 14441 N/m^2$, $T_{ci} = 936K$, and $U_{ci} = 2484 m/s$ (corresponding to a Mach number of 4.13).

4.2 Combustor Analytical Modeling

Once the combustor inflow conditions are obtained as shown above, the combustor itself was also analytically modelled as a constant area frictionless heat addition device using a single step solver which solved the continuity, momentum and energy equations combined with the equation of state to obtain the combustor outflow conditions, $P_{ce}, T_{ce}, \rho_{ce}, u_{ce}$. These equations are given below:

$$\rho_{ci} u_{ci} = \rho_{ce} u_{ce} \qquad (6)$$

$$P_{ci} + \rho_{ci} u_{ci}^2 = P_{ce} + \rho_{ce} u_{ce}^2 \qquad (7)$$

$$\left\{ \sum_{l=1}^{ncs} \alpha_l \left(h_{ref,l} + \int_{T_{ref}}^{T_{ci}} C_{P,l} dT \right) \right\} + \frac{u_{ci}^2}{2} + \frac{\dot{Q}_{comb}}{\dot{m}} =$$

$$\left\{ \sum_{l=1}^{ncs} \alpha_l \left(h_{ref,l} + \int_{T_{ref}}^{T_{ce}} C_{P,l} dT \right) \right\} + \frac{u_{ce}^2}{2} \qquad (8)$$

$$P_{ce} = \rho_{ce} R T_{ce} \qquad (9)$$

Here $\dot{Q}_{comb}$ is the energy rate to be added into the combustor for the various cases of interest. Four different energy rate amounts within the combustor were examined; first an initial 5.07 megawatts was added in the combustor for cases in which additional energy

rate amounts were distributed in the nozzle/afterbody flowfield (the unconventional cases). Furthermore, three conventional cases were examined with energy rate additions of 6.06, 6.57, and 7.07 megawatts in the combustor, corresponding to fuel-air ratios between 60-70% of the stoichiometric value for H2-air combustion. The distributed energy cases (the unconventional cases) were then examined for nozzle energy rate additions of one, one and a half, and two megawatts, which corresponded to the same total energy rates as the corresponding conventional cases (but with fifteen to thirty percent of the energy addition occurring in the nozzle/afterbody flowfield). Table 4.1 shows the combustor exit conditions computed for all four cases.

4.3 Methodology/Configurations for Parametric Study of Nozzle/Afterbody Flow

This study performed a parametric investigation of the effects of energy rate amount, energy deposition zone location, and zone area and zone aspect ratio on the vehicle performance. The configuration was defined such that a single energy deposition zone overlaid the grid in the region desired for energy deposition. For the parametric study,

Table 4.1: Final combustor exit conditions

	Distributed energy cases	Conventional 6.06 megawatts	Conventional 6.57 megawatts	Conventional 7.07 megawatts
P (N/m²)	52257	60911	65550	70415
T (K)	3000	3392	3592	3792
M	2	1.8	1.7	1.6
U (m/s)	2200	2134	2100	2063

twenty-one locations in the nozzle were selected such that they formed three lines of seven points each near the top, middle and bottom of the nozzle as shown in Figure 4.1. In this figure, each location is given an alphabetic designator to identify it. However, the four locations in the rear of the lower line had heating problems due to being in the cowl trailing edge wake and never ran successfully; furthermore some of the zones in the rear of the middle line showed no appreciable effect on the flow-field or resulting force and moment performance. Three different total energy rate amounts were examined by first adding five megawatts into the combustor as described above, then varying the energy rate amount (added downstream in the nozzle/afterbody flowfield) from one to two megawatts. Two different zone areas were examined, however the larger area had issues with physically intersecting the nozzle walls and hence was only analyzed for the middle (midstream) line of zones. The aspect ratio was defined as the height of the zone divided by the length of the zone, such that a higher aspect ratio corresponded to a taller zone. Two aspect ratios
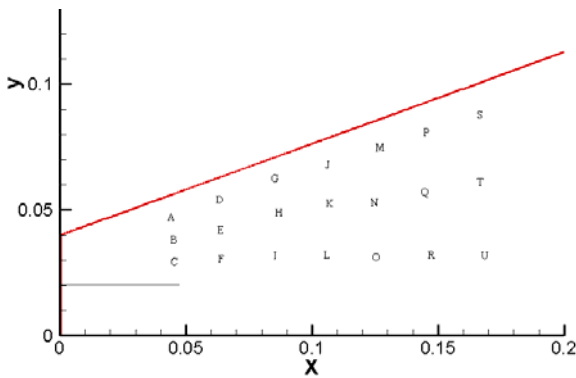

Fig. 4.1. Energy deposition zone locations

were examined; aspect ratio of 1.0 and 2.0. However the higher aspect ratio (taller zone) also had issues with the top line of zones intersecting the nozzle walls and hence was analyzed only for the middle (midstream) line of zones.

Grid convergence was checked by running a refined mesh (grid points doubled in each direction) for a representative case; changes in force, moment, and wall temperature distributions were less than 2%. Temporal convergence was ensured by running the code until the quantities of interest showed no further change.

The selected locations were first examined for the largest energy rate case and the smallest area with a square (aspect ratio of 1.0) zone. The cases which showed an improvement for those conditions were then examined for other energy rate amounts, zone areas and aspect ratio combinations. Table 4.2 shows a summary of the cases that were analyzed in this investigation.

4.4 Post-Processing and Analysis

After the CFD solutions were obtained for the parametric matrix shown above, it was necessary to use the pressure obtained from the simulations to compute an estimation of the axial force and pitching moment contribution of the nozzle/afterbody (for this study friction was not computed – due to the assumption of laminar flow in this particular study, the skin friction would be quite small). Furthermore, the adiabatic wall temperature (taken from the flow-field) was used in a comparative fashion to assess heating load characteristics of the various cases. The thrust force (and the lift force) on the nozzle was calculated by performing a summation (for nodes along the upper nozzle wall) of the pressures multiplied by the directed area they acted on, as shown in equations 10 and 11. The average pressure between two nodes was used and the area that the force operates on is the differential distance between the nodes.

$$F_x = \sum \frac{P_i + P_{i-1}}{2}(y_i - y_{i-1}) \qquad (10)$$

$$F_y = \sum \frac{P_i + P_{i-1}}{2}(x_i - x_{i-1}) \qquad (11)$$

The moments were calculated in a similar method, i.e. the average pressure

between two nodes was calculated then multiplied by both the directed area and the moment arm and the results were summed as shown in equation 12. The moments were

5.1 Effects of Energy Amount

The first group of cases reported on here is for selected ranges of energy amounts.

Table 4.2: Parametric cases

Energy Amount	Zone Area	Zone aspect ratio	Locations
1.0 MW	1.5 cm^2	1	A.B.C.D.E.F.G.H.I.J.K.M.P.S
		2	B.E.H.K.N
	5.0cm^2	1	B.E.H.K.N
		2	B,E,H,K,N
1.5 MW	1.5 cm^2	1	A.B.C.D.E.F.G.H.I.J.K.M.N.P.O.S.
		2	B.E.H.K.N
	5.0cm^2	1	B.E.H.K.N
		2	B,E,H,K,N
2.0 MW	1.5 cm^2	1	A.B.C.D.E.F.G.H.K.M.P.S
		2	B.E.H.K.N.O.T
	5.0cm^2	1	B.E.H.K.N.O.T
		2	B,E,H,K,N,Q,T

calculated referenced to the origin of the CFD grid, i.e. 0.02 m below the combustor exit, which is designated as x_m,y_m in equation 12 and are defined as positive when clockwise, i.e. positive moments imply a nose-up pitching moment. The moments on the nozzle/afterbody section are hence inherently negative.

$$M_m = \sum \frac{P_i + P_{i-1}}{2}((y_i - y_m)(y_i - y_{i-1}) + (x_i - x_m)(x_i - x_{i-1})) \quad (12)$$

5 Results of Parametric Nozzle/Afterbody Study

This section provides the results of the parametric study utilizing CFD of the nozzle/afterbody region of the flow-field. Effects on nozzle/afterbody flow-field structure and performance (force, moment, and wall temperature) are analyzed in terms of amount of energy rate added, size and shape of energy deposition zone, and location of zone.

An initial energy rate of five megawatts was added to the combustor and the forces and moment were calculated for this baseline case. Solutions were then obtained for cases in which an additional energy rate amount was added to the combustor (conventional) and to one of the downstream deposition zones (unconventional). The additional energy rate added in the nozzle region varied from approximately one to two megawatts (i.e. representing fifteen to thirty percent of the total energy added to the flow). The largest energy amounts were analyzed first; if the energy addition in a particular location did not appreciably affect the observed forces on the nozzle wall, any lower energy rate amounts were not further examined for that location.

Higher energies resulted in the largest pressures and temperatures in the energy deposition region due to the generation of a stronger shock wave, although some energy deposition locations in the nozzle were less sensitive to the energy amount, as will be discussed in the next section. The shock wave formed upstream of the energy deposition and

impacted the nozzle wall. This in turn caused a pressure spike that increased the forces and moments experienced by the vehicle surface. The shock wave also increased the temperature; however the majority of the heated flow from the energy deposition was entrained in the downstream flow without much thermal convection and did not impact the wall. Note that this is for laminar flow and it can be expected that turbulent flow will appreciably increase thermal diffusion with possible mitigation of this characteristic (i.e. turbulent flow will increase thermal diffusion such that the temperature rise may affect the wall upstream of the nozzle exit). For these cases, however, this had the effect of significantly reducing the temperature experienced by the nozzle walls. Figure 5.1 shows the effects of nozzle energy deposition on the pressure and temperature contours in the flow field for a selected case. The shock wave for the given case is seen to be formed along the front of the energy deposition zone and then curves back into the flow therefore intersecting the wall downstream of the energy deposition zone but well forward of engine exit.

The nozzle expansion causes the static pressure in the flow and hence the nozzle wall pressure to decrease very rapidly over the shoulder of the nozzle (at combustor exit) and as the flow moves through the nozzle (also due to the plume expansion process below the cowl), but the presence of the shock wave associated with energy addition forms a pressure spike at the location where the shock wave intersects the wall. The magnitude of this pressure spike is determined by the strength of the shock wave. Increasing the energy amount by half a megawatt strengthened the shock wave and raised the maximum pressure by approximately 20%, however without significantly affecting the location of the pressure spike. Figure 5.2 shows the wall pressure for all three energy amounts both for the conventional cases and in three selected zones in the nozzle. The behavior of the (upper nozzle) wall temperature is similar to that of the pressure. The temperature drops across the shoulder (at combustor exit) during the nozzle

expansion but of course increases across the shock wave associated with energy deposition. The core flow through the nozzle prevents the heated flow associated with energy deposition (or the flow which is affected by convective heat transfer from that zone) from impacting the nozzle wall which means that the temperature spike on the wall is primarily due to the heating from the shock wave. Since shock waves do not affect the temperature as much as the pressure, increasing the energy rate had less effect on the wall temperature than on the wall pressure, with temperature increases of approximately 100 K or only 1-2% for a deposited energy rate increase of half a megawatt. Figure 5.3 shows the wall temperature for all three energy amounts both for the conventional cases and in three selected zones in the nozzle.

The increased wall pressure due to the stronger shock wave caused the cases with higher energy rates added in the downstream zones to have significant force increases. An increase of half a megawatt in the energy rate in a given zone resulted in a 5-10% increase in the forces. However, the conventional approach of adding the energy in the combustor resulted in 5-10% higher forces than the nozzle energy addition, with the exact percentage varying since the forces for the unconventional case depended on the location of the energy deposition zone. Figure 5.4 shows the forces for the three conventional cases and for all three energy amounts in two of the nozzle energy deposition locations.

While the forces were lower for the cases with distributed energy in the nozzle (relative to the conventional all-combustor energy addition cases), the cases with nozzle energy addition for certain locations had significantly higher pitch-down moments. An energy rate increase of half a megawatt resulted in a 5-10% increase in the pitch-down moment for the nozzle energy deposition cases, again depending on the location of the energy deposition zone. Figure 5.5 shows the moments for both the three conventional cases and for all three energy amounts in two selected energy deposition locations in the nozzle.

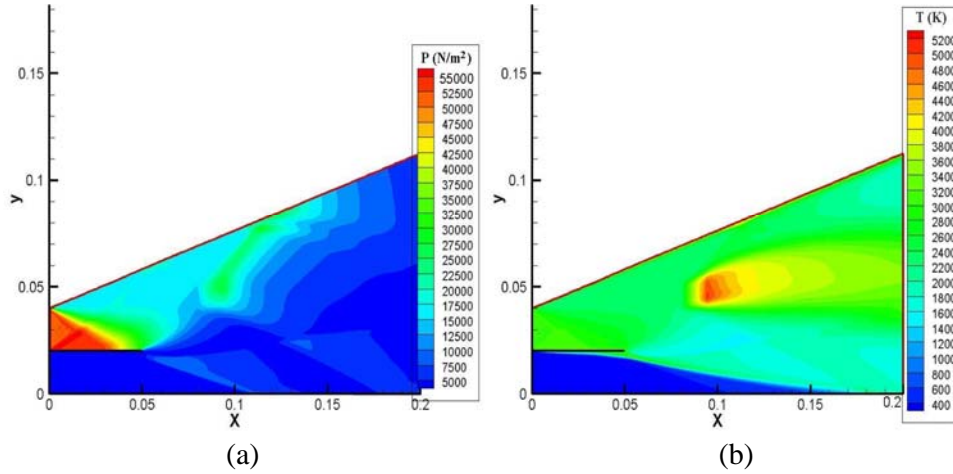(a)   (b)

Fig. 5.1. Flow contours for nozzle energy deposition, pressure(a) and temperature(b)
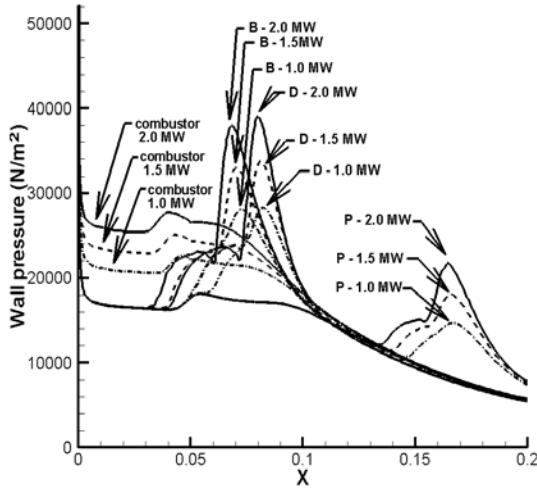

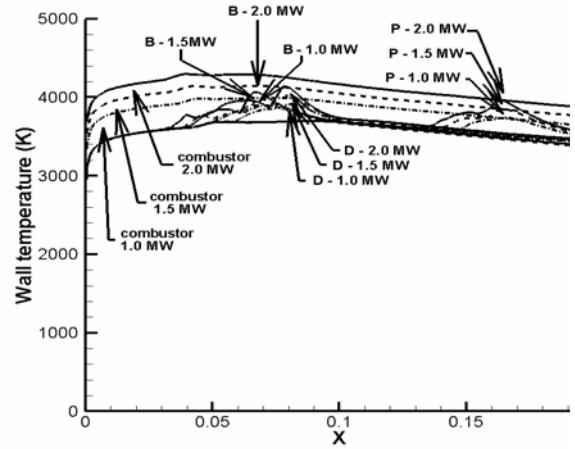Fig. 5.2. Wall pressure for selected points
with energy variation

Fig. 5.3. Wall temperature for
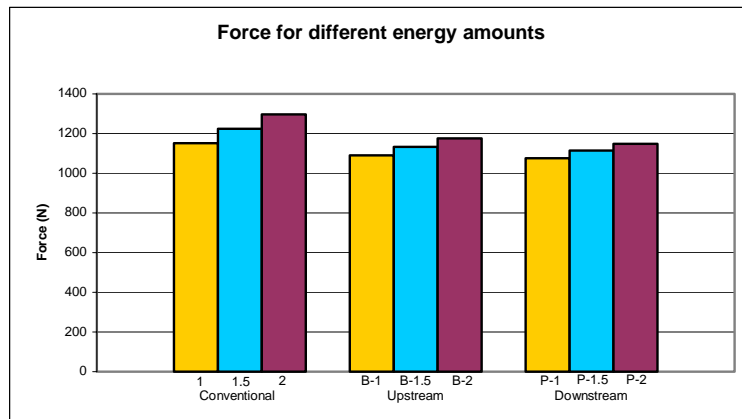selected points with energy variation
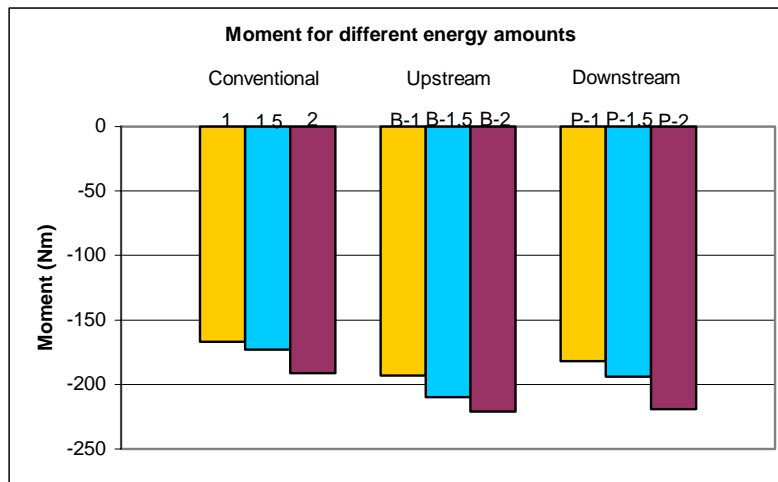

Fig. 5.4. Force for varying energy amounts

Fig. 5.5. Moment for varying energy amounts

5.2 Effects of Zone Location

In order to examine the impact of the zone location, a grid of zones was defined consisting of three lines, of seven points each, near the top, middle and bottom of the nozzle. The zones were defined to coincide with the grid lines which caused the zones to be quadrilateral since the grid lines are quadrilateral. Since the cowl was truncated 5 cm behind the combustor exit, the first column of zones was selected to be above the cowl while the rest of the zones were aft of the cowl trailing edge. Figure 5.6 shows a summary of the zones, the tested areas and aspect ratios. The zones near the front of the nozzle have some overlap so the zones were colored to help distinguish them. The top line of zones is blue, the middle line is black and the lower line is red. The larger areas and aspect ratios are only shown for the middle line of zones and are dark and light green respectively.

The four aft-most downstream locations on the bottom line of zones, locations L, O, R and U, had heating (high-temperature) problems due to being in the cowl wake. The flow patterns in these zones caused uneven heating in the energy deposition zone which resulted in some portions of the flow exceeding the temperature limits imposed by the thermodynamic modelling in the SPARK code; hence these locations could not be run successfully. The presence of the cowl had a

significant effect on the energized zones above it. Therefore the results for zones located above the cowl had several significant differences in comparison to results for zone locations aft of the cowl. In addition, several of the locations far downstream in the nozzle showed no appreciable performance effect since the shock wave did not actually intersect the wall; hence these locations were not examined for lower energy amounts.

The strength of the shock wave was controlled by the energy amount and not strongly affected by the energy deposition location. However, since the shock waves weakened as they extended outward from the heated zone, the shock waves from the middle and lower lines of zones had attenuated some of their strength by the time they intersected the wall and hence were not as strong as the shock waves from the top line of zones when they intersected the wall.

The upstream zones in the nozzle benefited from the higher pressures and temperatures in the flow exiting the combustor, this resulted in a larger maximum pressure. The zones near the aft end of the nozzle had longer moment arms but lower pressures due to the nozzle expansion process. The top line of zones had the largest pressure spikes, the middle line produced a somewhat smaller pressure spike due to the weakened shock, and the bottom line of zones had the smallest pressure spike. The angles associated with the shock waves resulted in the pressure spikes for the middle and lower
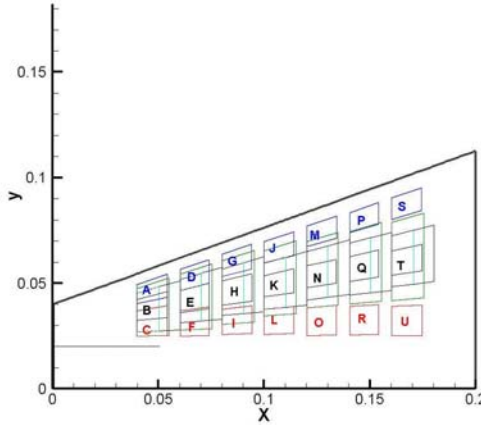
Fig. 5.6. Energy deposition zones

lines of zones being behind (aft of) the energy deposition zones. Figure 5.7 shows the wall pressure for the conventional case and for the various locations for an energy addition of 1.5MW, area of 1.5cm^2 and an aspect ratio of one. In this figure, the top line of zones are represented by solid lines, the middle line of zones by dashed lines and the lower line of zones use the dash dot pattern.

The maximum wall temperature was highest for the top line of zones, however even the temperature spike on the top line of zones had a maximum temperature that was comparable to the temperature of the conventional case, which means that the total heat transfer for a cooled wall would be significantly less (as the majority of the wall is 200-500 K cooler than the conventional case). Figure 5.8 shows the wall temperature for the conventional case and for the various zone location cases for an energy rate addition of 1.5MW, area of 1.5cm^2 and an aspect ratio of one; the top line of zones are represented by solid lines, the middle line of zones are dashed lines and the lower line of zones use the dash dot pattern.

The energy deposition increased the forces as a result of the pressurization from the shock wave, although the conventional cases had larger forces due to the higher average pressure at combustor exit. The forces were not strongly affected by the presence of the cowl although the increased pressurization from the

cowl did increase the forces slightly for the zones located above it. The largest forces occurred with energy addition in the zones near the top wall since they had the largest maximum pressures. The zones associated with the middle line had less impact while the lowest zones had minimal effect (due to the low maximum pressure). The forces decreased for the zones that were further downstream. Figure 5.9 shows the forces for the conventional case and for cases with different zone locations for an energy rate addition of 1.5MW, area of 1.5cm^2 and an aspect ratio of one. Here the top line of zones are represented by the blue bars, the middle line of zones by black bars and the lower line of zones are represented by red bars.

The moments were largely determined by a combination of the pressure and the moment arm which meant that the moments varied significantly more than the forces (due to the pressure spike phenomena on the aft side of the nozzle wall associated with downstream energization). The moments were taken around the origin of the CFD grid i.e. 0.02 m below the combustor exit, hence the moment arm lengthened the farther downstream the pressure spike occurred. The pressure spike was highest for cases with energization near the front of the nozzle; however the moment arm was largest for cases with energization located in the aft flow-field of the nozzle. In general, the top line of zones performed the best due to the higher pressure from the stronger shock. The exception was location A which was the most forward location along the top wall; it simply did not have a long enough moment arm to generate a large moment. The case that corresponds to energy in location B (i.e. below that of A) performed better in terms of moment production due to the pressure spike which occurred further downstream. (This resulted from the shock angle and transit to wall). The cases corresponding to energization of the middle line of zones performed better in terms of moment than those associated with the lower
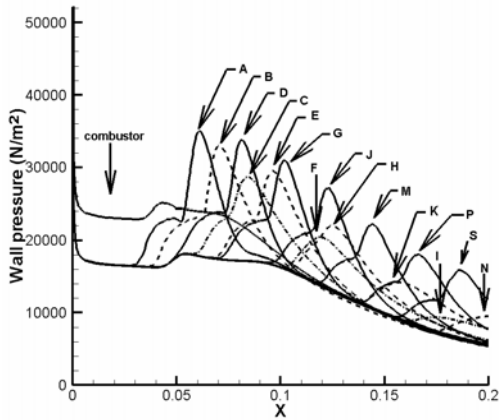
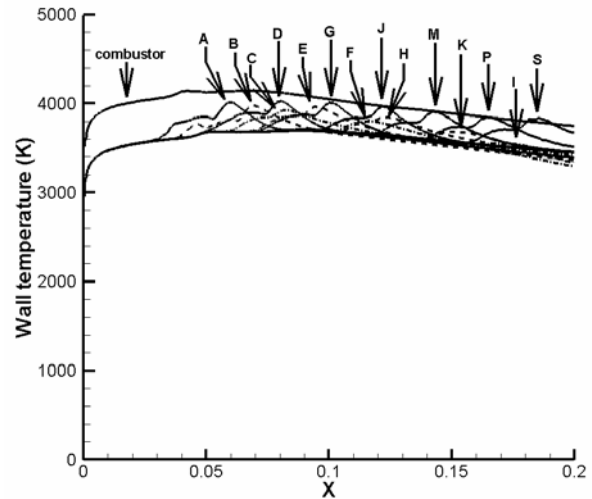Fig. 5.7. Wall pressure for various zone locations

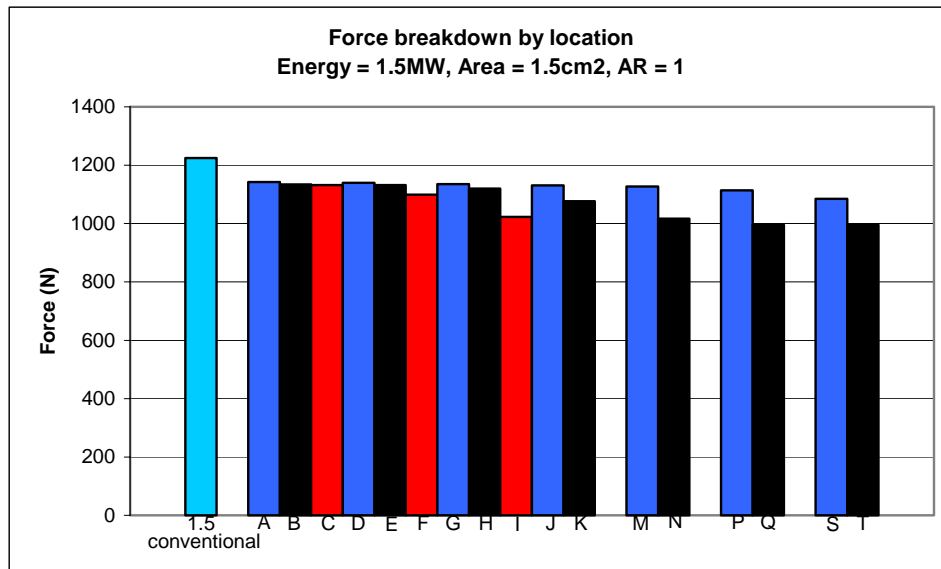
Fig. 5.8. Wall temperature for zone locations

Fig. 5.9. Forces for various locations

line of zones due to the shock being stronger when it intersected the nozzle wall.

The three locations in which energization generated the largest nose-down moments (and hence were regarded as the optimal cases) were locations B, D and P. Location B, which was located in the middle line of zones just over the cowl, benefited both from the increased pressurization from the cowl and the already high pressures and temperatures coming out of the combustor; it in fact had the largest moment for the cases examined. This case performed better than the case for heating of zone A above it because the pressure spike was farther aft which resulted in a larger moment arm. Locations D (directly behind the cowl along the top line of zones), and P (approximately three-fourths of the way

aft along the top line) had the next largest favourable effect on the moment. Location D benefited from the higher pressures and temperatures associated with the proximity of the combustor, while location P had lower pressures due to the nozzle expansion process but benefited from a long moment arm. Location S had the longest moment arm but the pressure spike was not entirely on the nozzle wall which reduced the effects significantly. The moment for location D was less sensitive to the energy rate variation then for location P, so location D performed better for the lower energy rates; conversely location P performed better for the higher energy rates. Figure 5.10 shows a summary comparison of the moments for the cases associated with the three 'optimal' locations with the corresponding conventional cases at the three total energy rates studied. The moment for energy added in location B was 15-20% higher than the conventional case. The moment for energy added in location D was approximately 10% higher than the conventional case. The moment for energy added at location P was 8-14% higher than the conventional case. The axial forces for all locations were between 7-9% less than the conventional cases as discussed earlier the upstream zones had larger forces, hence the moments for energy addition in locations B and D were 7% less than the conventional case and the moment for energy added in location P was 9% less than the conventional case.

5.3 Effects of Zone Area

The zone area strongly affects the maximum temperature in the flow, since this temperature occurs at the end of the energy deposition zone. A smaller area will result in a higher temperature; therefore the temperature limits on the thermodynamic curve fits in the Spark code also factored into the determination of the minimum area studied here. The larger area had a smaller selection of locations since the top and bottom lines of zones intersected the wall when the area was increased. The middle line of zones was fully tested and the trends were examined.

The smaller area was selected to be 1.5 cm^2, and the larger area was selected to be 4 cm^2, the angle of the grid lines meant that the aft end of the zone was taller than the front; this effect caused the zone areas to vary slightly from the selected area. The smaller area was examined first, and cases which demonstrated no appreciable effect on performance were then not examined for larger energized areas.

Increasing the zone area generally resulted in a weaker shock with a larger shock angle. The downstream zones were less sensitive to the area variation because they had a higher Mach number entering the heated zone than the upstream zones. This tended to strengthen the downstream shocks for those cases.

Since increasing the zone area weakened the shock wave in general, the maximum pressure on the wall was reduced by 15-20% for all cases examined here. The effect was relatively stronger in the upstream zones since the upstream shocks were more sensitive to the area variation (again due to the lower Mach number). Figure 5.11 shows the wall pressures for cases from the zone area variation study and compares the pressures to the conventional case. Here the zones have aspect ratios of 1.0 with an energy rate addition of 2 MW. The smaller zone areas are represented by solid lines and the larger areas by dashed lines.

The increase in the area of the energized zones also reduced the maximum temperature by 2-4%, due to the weaker shock wave. The reduction in the temperature was less significant for the cases of energization in the downstream zones, again due to the shock wave's lower sensitivity to the heated zone area in the aft parts of the nozzle flow-field. Figure 5.12 shows the wall temperature for the area variation for zones with an aspect ratio of 1.0 and an energy addition of 2 MW. Also shown is the nozzle wall temperature for the conventional case. Here the cases with smaller zone areas are represented by solid lines and the larger area cases are represented by dashed lines.
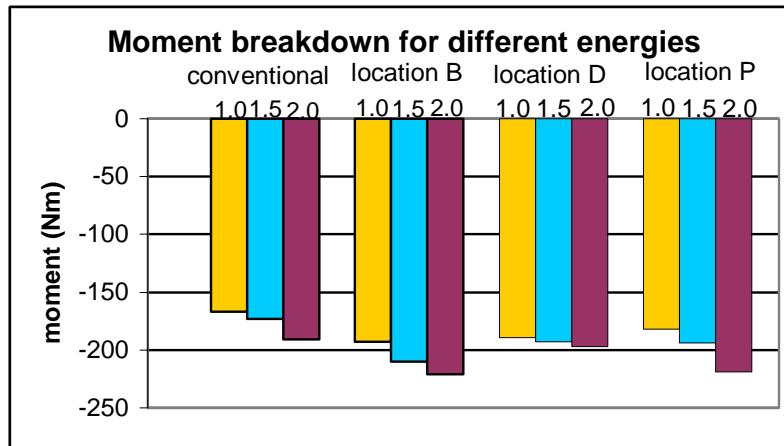
Fig. 5.10. Moment breakdown by energy amount for optimal locations

Since the area increase lowered the wall pressure, it also caused a slight reduction in the axial force, as demonstrated in Figure 5.13 which shows a comparison of the forces obtained for cases in which the area is varied (again aspect ratio of 1.0 with energy rate addition of 2 MW); also shown is the axial force for the conventional case.

Increasing the area of the energized zone also decreased the moment by 7-10% for all cases with the exception of location H, as demonstrated in Figure 5.14. This figure shows a comparison of the forces obtained for the area variation study (along with the conventional case) for zones with an aspect ratio of 1.0 and energy rate addition of 2 MW.

Location H was an exception due to its axial position near the middle of the nozzle. As discussed previously in the location study results, the moment for cases with energization in the forward part of the nozzle was dominated by the pressure while the moment for cases with aft energization was dominated by the moment arm of the pressure spike. This indicates that the moment for the zones in the middle line are less sensitive to the area variation; therefore the moment for energization at location H was not significantly affected by the area change.

Two of the three optimal locations previously determined in the location study could not be examined for the area variation because the higher area caused the zones to intersect the nozzle wall. The third optimal location was examined for the increased area and showed an 8% reduction in the moment with only a 4% reduction in the temperature. This was similar in trend to the other cases examined. Therefore the smaller area is considered to be a better option for energy deposition due to the stronger moment generated.

5.4 Effects of Zone Aspect Ratio

The aspect ratio was defined as the height of the energized zone divided by its length, so a higher aspect ratio corresponded to a 'taller' zone. The selected aspect ratios were an (approximately) square zone, which corresponded to an aspect ratio of one, and a zone that was twice as tall as it was long, which corresponded to an aspect ratio of two. Decreasing the aspect ratio to create a zone that was longer than it was tall resulted in the flow temperature at the end of the energy deposition zones exceeding the temperature limits imposed by the curve fits in the SPARK code, hence those cases could not be examined. The larger aspect ratio caused the top and bottom lines of zones to intersect the wall, so only the middle zones were examined.

The increase in the aspect ratio of the energized zones affected the strength and angle of the shock wave by generally causing a weaker shock (less energy per area) with a larger normal component (front of the shock) in
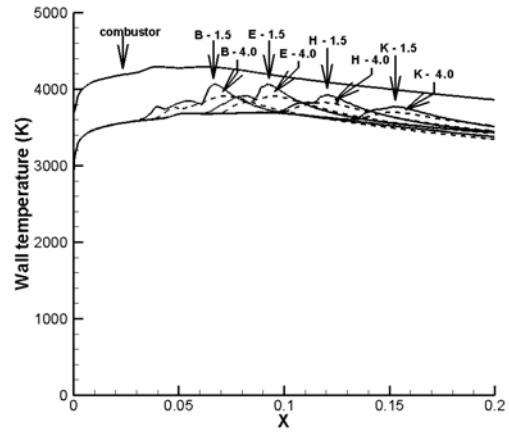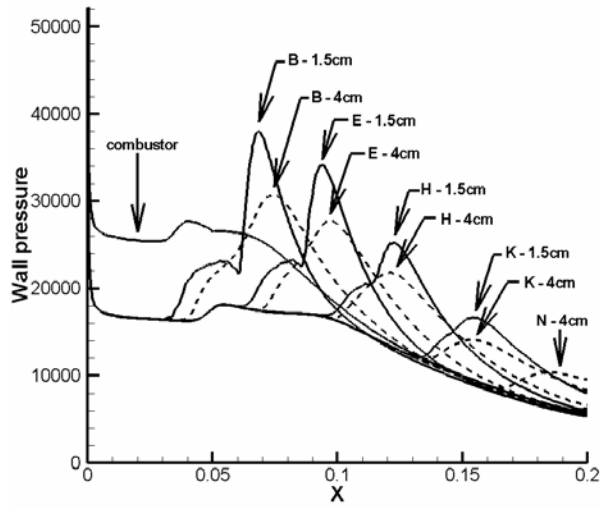
Fig. 5.11. Wall pressure for area change

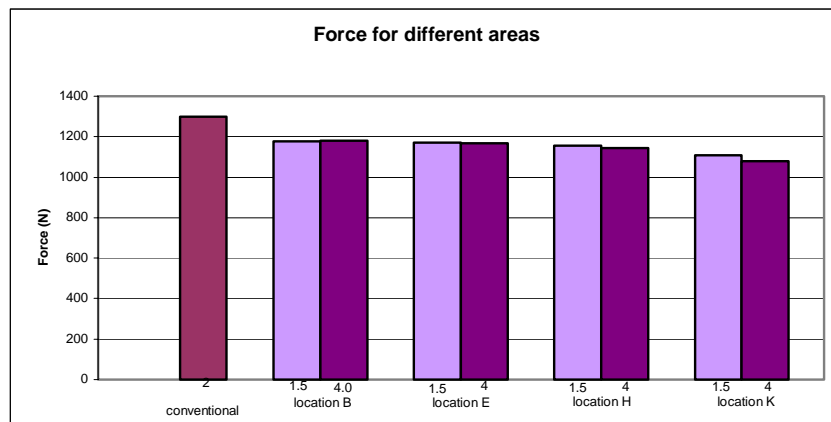Fig 5.12. Wall temperature for area change
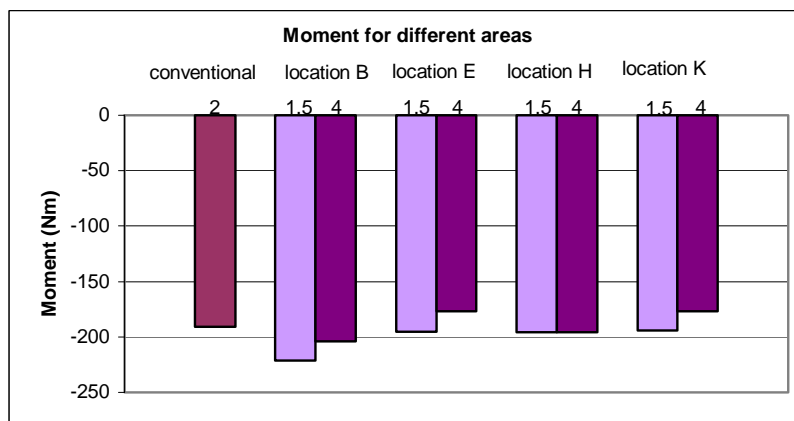

Fig. 5.13. Force breakdown for area variation

Fig. 5.14. Moment breakdown for area variation

front of the energy deposition zone; the shock then tapered off into an oblique shock at approximately the same angle as for the lower aspect ratio cases. The increase in the normal spatial component of the shock wave caused the shock wave to intersect the wall upstream of the original location.

The combination of the weaker shock and the movement of the point where it contacted the wall meant that increasing the aspect ratio of the energized zones decreased the maximum pressure on the wall by 3-15% and additionally caused the location of the pressure spike to move upstream. The reduction in the maximum pressure was less significant for the cases with energization in the downstream zones due to the higher Mach number entering those zones. Figure 5.15 shows the wall pressure for the conventional case and for the cases with the aspect ratio variation of the downstream energized zones with an area of 1.5 cm^2, an energy rate addition of 2 MW. Here the case with the smaller aspect ratio is represented by the solid lines and the taller aspect ratio is represented by the dashed lines.

The temperature behaved similarly to the pressure, i.e. increasing the aspect ratio decreased the maximum temperature by 1-3% and shifted the location of the maximum temperature on the nozzle wall farther upstream. Figure 5.16 shows the wall temperature distribution for the conventional case and for the cases with aspect ratio variation with an area of 1.5 cm^2 and an energy addition of 2 MW. Again, the smaller aspect ratio case is represented by the solid lines and the taller aspect ratio is represented by the dashed lines on this figure.

The reduction in the maximum pressure reduced the moment by 4-7% in most cases. Location H was an exception. Due to the movement of the pressure spike, this case actually provided a 2% larger moment. Figure 5.17 shows the moments for the conventional case and for cases with aspect ratio variation in the downstream energized zones with a zone area of 1.5 cm^2 and an energy rate addition of 2

MW. Here the darker bars represent results for the taller zones (higher aspect ratio zones).

The effect on the forces was less significant with a slight reduction of less than 1% for the larger aspect ratio (taller) zones. Figure 5.18 shows the forces for the conventional case and for the cases with aspect ratio variation with an area of 1.5 cm^2 and an energy rate addition of 2 MW. Again the darker bars correspond to the taller zones.

As noted earlier, two of the optimal locations determined previously in the location study were on the top line of zones and thus could not be examined for the aspect ratio variation. The third location was examined and the higher aspect ratio was not beneficial. Based on the trends for the middle line of zones, increasing the aspect ratio would likely be counterproductive for the other two locations as well since the aspect ratio increase lowered the performance, and the zones would need to be shifted down, which would also lower the effects as determined from the location study.

6 Overall Propulsion Flow-Path Effects

6.1 Calculation of Inlet, Forebody and Combustor Pitching Moment

This section describes the analytical estimation strategy and results for the pitching moment contribution (to the overall vehicle pitching moment) associated with the modelled propulsive flowpath, here specifically from inlet face to combustor exit. Results obtained from this analysis will then be incorporated with the computational results obtained in the previously described parametric CFD study, which provided wall integrated moments and forces from combustor exit to vehicle tail for the distributed energy concept studied here. The analytical strategy for estimation of the nose to combustor exit pitching moment is based on the direct calculation of the pitching moment on the surfaces of an appropriately defined control volume (see earlier sections) using the moment of momentum equation. This relationship (for this case) is a
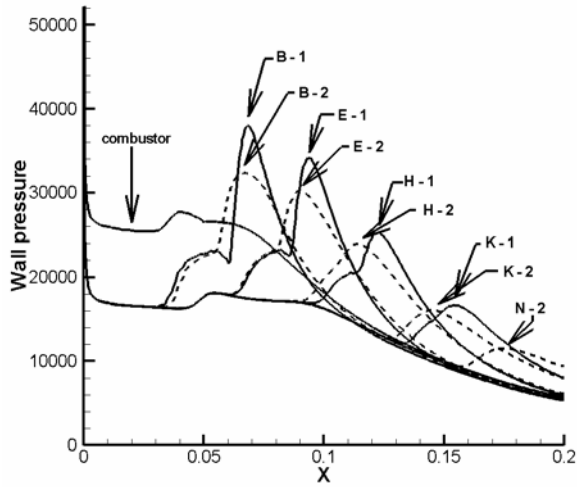
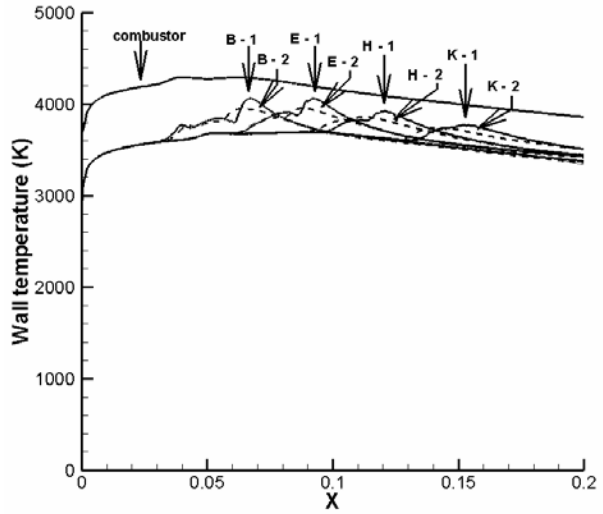Fig. 5.15. Wall pressure for AR change

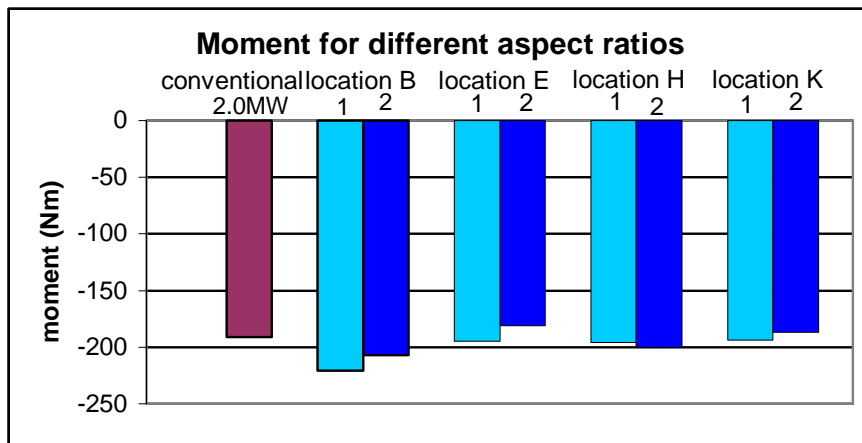Fig. 5.16. Wall temperature for AR change

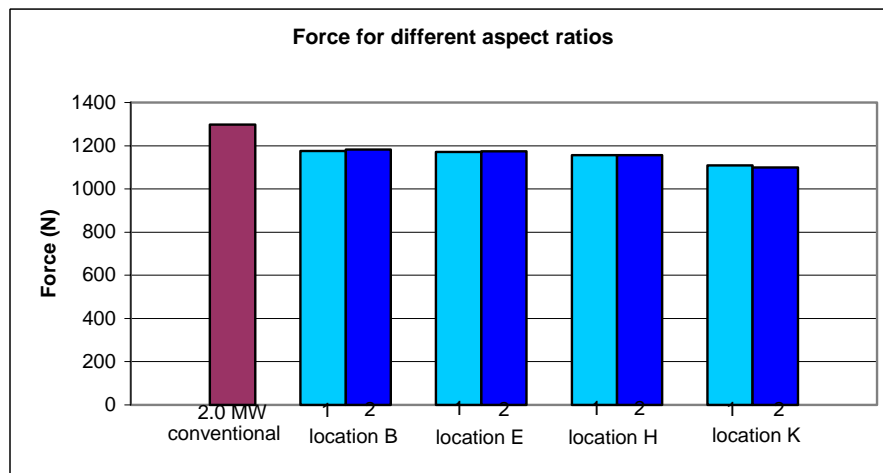Fig. 5.17. Moment breakdown for aspect ratio variation

Fig. 5.18. Force breakdown for aspect ratio variation

function of the known combustor exit conditions used in this study and the engine inflow conditions at the flight condition of interest.

The general form of the moment-of-momentum theorem for steady flow is as follows:

$$\sum \hat{R} \ x \ \hat{F} = \int_{S} \rho \ (\hat{R} \ x \ \vec{V}) \ (\vec{V} \bullet \hat{n}) \, dS \qquad (13)$$

Here S is the surface of some control volume of interest, $\vec{V}$ is the velocity vector, $\hat{R}$ is the position vector from the point from which moments are to be measured, $\hat{F}$ is the force vector and $\hat{n}$ is the unit normal directed pointing out from the control volume. The left hand side of this equation represents the moments acting on the fluid in the control volume.

Consider the sketch shown in Figure 6.1 for the 2-D generic vehicle shape of interest in this study. If one defines a control volume (as shown) encompassing the inlet face plane, the forebody/inlet surfaces, the bottom plane including the cowl surface, the wetted surfaces of the combustor, and the combustor exit plane, the moment-of-momentum theorem can be applied to this with equation 14 as the result for the pitching moment on the control volume:

$$M_{m_{pitch}} = \int_{A_{ce}} [\rho uv(x - x_m) - (\rho u^2) \ (y - y_m)] \, dA_{ce} -$$
$$\int_{A_i} [\rho uv(x - x_m) - (\rho u^2) \ (y - y_m)] \, dA_i$$
$$(14)$$

In the problem of interest, there is no non-uniformity on inlet face or combustor exit plane (one-dimensional flow) and there is no y component of velocity (no v component). Hence the expression (per meter depth for 2-D) becomes:

$$M_m = \int_{A_{ce}} -(\rho u^2)_{ce} \ (y - y_m) dy + \int_{A_i} (\rho u^2)_i \ (y - y_m) dy$$
$$(15)$$

This is equal to the pitching moment as referenced from a defined point (x_m, y_m) due to forces and moment arms on *all* surfaces of the defined control volume. This

implicitly includes the moment caused by the pressure forces on the inflow and outflow planes which is not felt by the engine, therefore, in order to obtain the moment on only the side surfaces of the control volume (corresponding to the surfaces coincident with the inlet upper surface and the cowl wetted surface of the actual vehicle), the moments associated with the force due to pressure on inflow and outflow planes of the control volume (i and ce) must also be removed from this term. Note also that this formulation is an estimation because it does not account for the fact that the cowl leading edge is generally located somewhat downstream of the axial location of the inlet face (i.e. the present formulation assumes a cowl leading edge all the way forward to the inlet face plane for the moment calculation). However, in general, the contribution from this approximation is very small.

The height of the captured streamtube at inlet face is 0.054012 m while the height of the combustor exit is 0.02 m. The reference point (m) for the moment calculation is taken as the origin of the CFD grid i.e. 0.02 m below the combustor exit. Evaluating this moment and correcting for the contributions of pressure on inflow and outflow (see above discussion), the moment on the forebody/inlet/combustor can then be directly computed as 143.6 N-m/meter (width) for all energy cases. The change in the moment between the different combustor heat addition cases is negligible because the combustor was modeled as inviscid and conserved the stream thrust. The axial (drag) force on the propulsive flowpath from inlet face (i) to combustor exit (ce) is also the same for all four cases (due to one-dimensional modeling of inviscid flow in the combustor); that value is 531.96 N (drag), as calculated from the change in stream thrust from inlet face to combustor exit.

There are several important points regarding this estimated value of pitching moment for the front part of the propulsive flow path. It is somewhat small (relative to
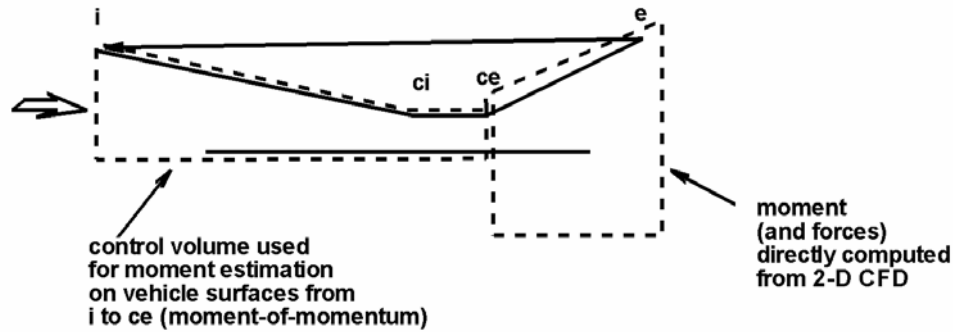
Fig. 6.1. Sketch of vehicle configuration showing control volume used for moment calculation

the nose-down moments directly integrated in the parametric study of the nozzle/afterbody) because the angle of attack for this study was taken as zero. As the angle of attack of the vehicle increases (typical angle of attack ranges may be up to 4 to 6 degrees), the pitch up moment magnitude associated with the inlet/forebody/combustor would increase significantly. In addition, the contraction ratio for this vehicle (area of captured stream tube to area of combustor entrance) is very small due to the specifics of the selection of the model made in this study. Future studies of the concept of energy distribution in the combustor/nozzle/afterbody need to incorporate angle of attack studies and entire nose to tail CFD simulations with more realistic contraction ratios.

6.2 Overall Propulsive Flow Path Pitching Moments and Forces

After obtaining the forces and moments for the vehicle forebody, the best cases from the parametric study were examined in terms of the overall effect on the propulsion flowpath. Due to the vehicle having an angle of attack of zero degrees, the nose-up moment from the forebody was smaller than for a typical vehicle which would fly at a higher angle of attack. This resulted in the total moment for the simulated cases being in the nose-down direction, which is not typical.

Including the forebody effects magnified the differences between the conventional and unconventional cases. The thrust from the distributed energy cases went from 7-9% less than the conventional cases for only considering the nozzle, to 15-20% less for the overall effect. The effect on the moments was also magnified; the distributed energy cases went from 15-20% higher than the conventional cases to being 50-125% higher for the overall effect. Table 6.1 summarizes the overall engine forces and moments for the conventional and optimal distributed energy cases and gives the percent difference between the moments for the conventional and distributed energy cases.

Figure 6.2 shows the overall engine thrust for the conventional and optimal distributed energy cases. The reduction in the thrust for the distributed energy cases is significant, but the overall thrust is still large enough to allow the vehicle to perform well and even accelerate under these conditions.

Figure 6.3 shows the overall moment on the engine for the conventional and optimal distributed energy cases. The moments for energy deposition at location B are all greater than for the conventional case with 7MW of energy addition, indicating that it is possible to reduce the amount of fuel significantly and still have a strong nose-down moment. The moment for energy deposition at location D is smaller than for location B, but larger than the corresponding conventional cases. Energy deposition at location P near the exit of the nozzle also causes a strong moment, although it responds better to the higher energy amounts.

Table 6.1: Overall thrust and moment

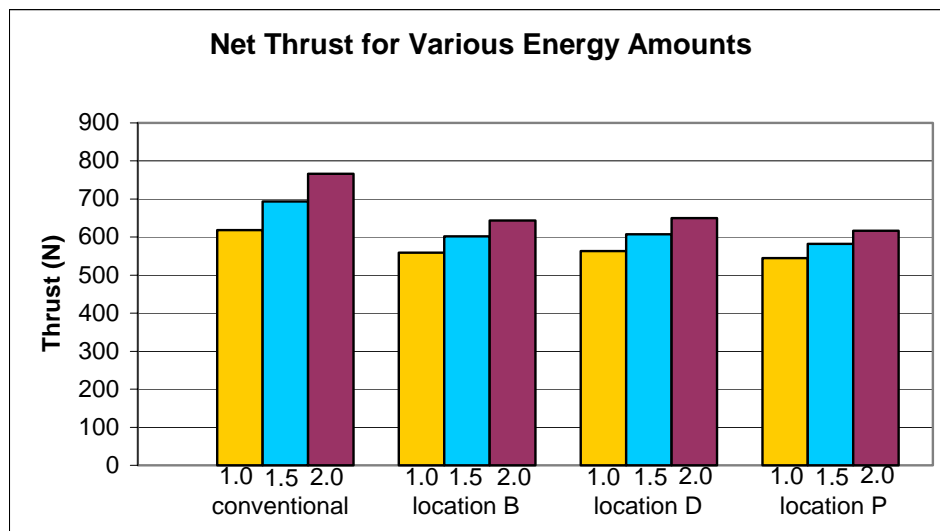|	Thrust	Moment	M% difference
7MW conventional	766.157	-47.4	
B – 2MW	644.03451	-77.4	63.29
D – 2MW	649.90633	-53.4	12.66
P – 2MW	616.48421	-75.4	59.07
6.5MW conventional	693.37521	-29.4	
B – 1.5MW	602.20113	-66.4	125.85
D – 1.5MW	607.45321	-49.4	68.03
P – 1.5MW	581.85763	-50.4	71.43
6.0MW conventional	618.8	-23.4	
B – 1MW	559.18	-49.4	111.11
D-1MW	562.93	-45.4	94.02
P-1MW	544.84	-38.4	64.10

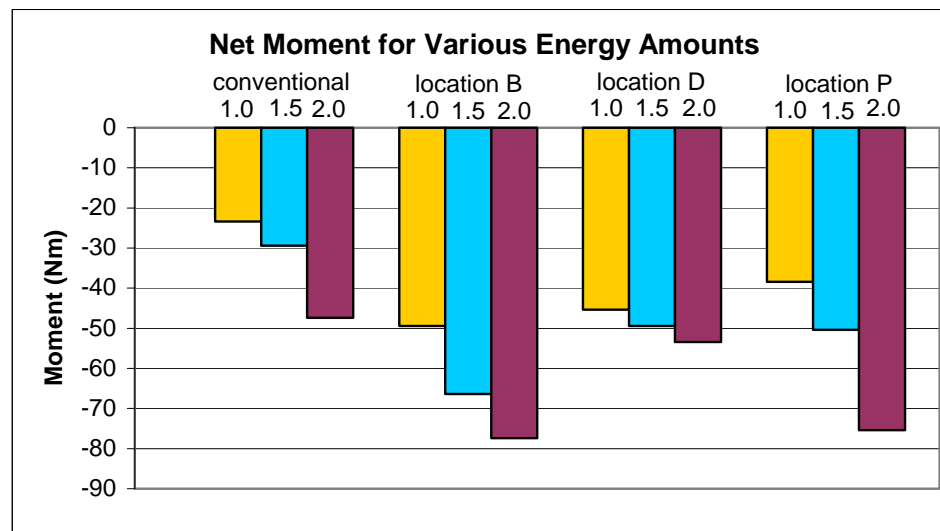Fig. 6.2. Thrust comparison for the overall engine

Fig. 6.3. Moment comparison for the overall engine

7 System Applications

The preceding sections presented results of analyses to show the effectiveness of energy deposition in the nozzle exhaust region for moment control and heat balancing through the engine. Ultimately it is necessary to determine the benefits of such technology (if deemed feasible for further analysis) as applied to an entire system (aerospace vehicle). Design 'penalties' include the additional weight and the efficiency of the device required to accomplish the deposition. These would be traded against the system benefits, such as reduced weight in the combustor/nozzle due to less heat load, more favorable moments which would reduce ballasting needs. Based on the data obtained in this investigation, an example system effectiveness (effectiveness of energy transmission into the flow-field) can be examined versus percent decreases in engine thrust, increases in engine pitch down moment, and an *estimated* percent reduction in overall combustor/nozzle heat transfer, all measured from the nominal case with no energy distribution – i.e. all energy added in

the method for increasing the nose-down moment while the reduction in combustor weight due to reduced thermal loads would tend to help increase the nose-down pitching moment. Obviously, it is necessary to study the system-level ramifications of such a technique as explored here before making definitive conclusions as to its feasibility or lack thereof.

8 Conclusions

This study examined the effects of focused energy deposition in the nozzle of a waverider travelling in hypersonic flight at Mach 9 at ambient conditions corresponding to an altitude of 30 km. The study modelled the vehicle forebody and combustor analytically and performed a parametric numerical survey of the effects of energy deposition in the vehicle nozzle/afterbody and examined the effects of the energy deposition amount, energy deposition zone location, energy deposition zone area and energy deposition zone aspect ratio.

The forebody was modelled as adiabatic with a large total pressure loss to

Table 7.1 Energy deposition effectiveness estimation

η	$\% \, \Delta Thrust$	$\% \, \Delta Moment$	$\% \, Heat-transfer$
100	-16	63.2	80
75	-21.4	40	78
50	-27	4.2	76
0	-37.4	-36	73

the combustor). This data (including estimated heat transfer from predicted wall temperatures and extrapolated data at 0% effectiveness) is shown in Table 7.1.

This table indicates that, for the configuration analyzed in the present study, there is little use in considering the technique for effectiveness less than 50%, unless the reduction in heat transfer results in enough weight savings to counter the thrust decrease. Note that the addition of subsystems for energy deposition in the rear of the vehicle would also tend to reduce the effectiveness of

account for the shock system; the inlet contraction ratio was chosen as less than 3 to allow for more variation in the amount of energy added to the flow in either the combustor or nozzle. The combustor was modelled as an inviscid constant area heat addition; there were four different combustor energy amounts examined, corresponding to three conventional cases and the combustor for the distributed energy cases. The nozzle/afterbody was modelled using CFD and included the interactions between the exhaust and the flow underneath the body.

The flow was modelled throughout the engine as heated air and did not include chemical reactions, although the temperature dependence of the specific heat was included in the model.

The energy deposition in the nozzle was strongly affected by the energy deposition amount, the energy deposition zone location, the energy deposition zone area and the energy deposition zone aspect ratio. Increasing the energy increased the moment more than it increased the temperature, so higher energies are viewed as beneficial. The effects of the zone location were more complicated; in general, locations near the top wall had the best performance. Upstream and downstream zones performed better than zones in the middle of the nozzle, although moving the zone too far upstream reduced the moment arm and significantly reduced the moment. Increasing the zone area reduced the force and moment more than it reduced the temperature, hence smaller areas are preferred. Adjusting the aspect ratio to make the zone taller also reduced the force and moment more than it reduced the temperature, so short zones are preferred.

The results of this study show a definite potential for utilizing energy deposition in the nozzle or afterbody to optimize the overall vehicle performance. All cases had a significant temperature reduction with the majority of the nozzle being 500 K or 10-15% cooler than the case where the energy was entirely added in the combustor. The optimal cases also showed a significant moment improvement of 15-25% when just examining the nozzle although all nozzle energy deposition cases had 5-10% lower forces than the combustor energy addition. When the overall effect on the engine was examined, the optimal distributed energy cases had moment increases of 50-125% and force reductions of 15-20% compared to the conventional cases.

A small zone with a large energy amount located either near the front or back of the nozzle along the top wall, or in the middle above the cowl appears to be the optimum configuration. This method can produce an additional 15-25% more moment in the nozzle, which can increase the overall engine moment by 50-125%, to assist in vehicle stability and lower the nozzle wall temperature by 200-500K thereby significantly reducing the heating load on the vehicle. Nozzle energy deposition does result in a 5-10% loss in the force produced in the nozzle, corresponding to a 15-20% overall reduction in thrust, however the improved stability would reduce the necessary control surface deflection and probably lower the weight which would reduce the drag and could offset the lower thrust.

The benefits in terms of favourable moment characteristics and indication of possible reductions in (propulsion system) heat transfer due to the optimal distribution of energy in the nozzle flow-field are shown in this work to be significant, and may result in the ability to reduce the overall vehicle weight, i.e. provide entire system-level benefits for high-speed vehicles. This in turn would reduce the drag and may compensate for the reduction in the thrust of the propulsion system, depending on the specific vehicle involved.

There is a significant amount of future work that should be done to expand on the work done in this paper on the topic of distributed energy deposition. It would be useful to examine the impact of turbulence and include the skin friction in the force analysis since it would be more significant in a turbulent study. Future studies should also examine the effects of air chemistry and specifically model the effects of disassociation in the flow, as well as model fuel injection, mixing and chemical combustion in the combustor, instead of as a simple heat addition in the combustor as done in the present study. A more detailed modelling and simulation of the vehicle that examined the effects of the vehicle angle of attack and incorporated a CFD model of the forebody (i.e. with a more realistic contraction ratio) would be beneficial. Also, the use of a non-adiabatic wall in the CFD

modelling would enable the computation of the actual heat transfer for a cooled wall. Finally, full system level studies should include the effect of the innovations on the vehicle weight and the required wing area.

Acknowledgements

The authors would like to thank Dr. José Camberos of the Air Force Research Laboratory. Thanks are due to the Air Force Office of Scientific Research for support under the auspices of the AFRL Summer Research Program during 2007.

References

[1] Mehta, U.B. Air-breathing aerospace plane development essential: hypersonic propulsion flight tests. *NASA Technical Memorandum 108857*, November 1994.

[2] Dornheim, M. A. X-43 flight test indicates thrust is greater than drag. Aviation Week. April 2004.

[3] McClinton, C. R. X-43 scramjet power breaks the hypersonic barrier; Dryden Lectureship in research for 2006 (AIAA archives). January, 2006.

[4] Khamooshi, A., Taylor, T., Riggins, D.W. Innovative concepts for large-scale drag and heat transfer reduction in high-speed flows. *AIAA Journal*, Vol. 45, No. 10, pp. 2401-2413, 2007.

[5] Riggins, D., Taylor, T., Moorhouse, D., Terhune, L. Methods for the design of energy efficient high-speed aerospace vehicles, *Aeronautical Journal of the Royal Aeronautical Society*, pp 297-309, 2007.

[6] Knight, D. Survey of aerodynamic flow control at high speed by energy deposition. AIAA Paper 2003-0525, January 2003.

[7] Marconi, F. An investigation of tailored upstream heating for sonic boom and drag reduction. AIAA Paper 98-0333, January 1998.

[8] Riggins, D.W., Nelson, H. F., and Johnson, E. Blunt body wave drag reduction using focused energy deposition. *AIAA Journal*, Vol. 37, No. 4, pp. 460-504, 1998.

[9] Froning, H.D. and Roach, R.L. Application of CFD to problem of drag reduction by free stream perturbations. AIAA Paper 98-2655, June 1998.

[10] Riggins, D.W., Barnett, J.T., and Taylor, T. Drag reduction and heat transfer mitigation for blunt bodies in hypersonic flight – a survey of techniques. AIAA Paper 2003-6968, 2003.

[11] Khamooshi, A. *Numerical investigation of the effects of coupling upstream energy deposition and forward-facing injection on a blunt body in Mach 10 flight*. Masters Thesis, University of Missouri – Rolla, 2005.

[12] Riggins, D., Taylor, T., and Moorhouse, D. Methodology for performance analysis of aerospace vehicles using the laws of thermodynamics, *AIAA Journal of Aircraft*, Vol. 43, No. 4, pp. 953-963, 2006.

[13] Drummond, J.P., Rogers, R.C. and Hussaini, M.Y. A detailed numerical model of a supersonic reacting mixing layer. AIAA Paper 86-1427, June 1986.

[14] McBride, B. J. and Gordon, S. and Reno, M. A. Coefficients for calculating thermodynamic and transport properties of individual species. *NASA TM 4513*, October 1993.

Copyright Statement